Atmos. Meas. Tech. Discuss., 5, 8789–8813, 2012
www.atmos-meas-tech-discuss.net/5/8789/2012/
doi:10.5194/amtd-5-8789-2012

Atmospheric Measurement Techniques Discussions

Note on rotational-Raman scattering in the O_2 A- and B-bands: implications for retrieval of trace-gas concentrations and terrestrial chlorophyll fluorescence

A. Vasilkov[1], **J. Joiner**[2], **and R. Spurr**[3]

[1]Science Systems and Applications Inc., Lanham, MD, USA
[2]NASA Goddard Space Flight Center, Greenbelt, MD, USA
[3]RT Solutions Inc., Cambridge, MA, USA

Received: 29 November 2012 – Accepted: 10 December 2012
– Published: 13 December 2012

Correspondence to: A. Vasilkov (alexander.vasilkov@ssaihq.com)

Published by Copernicus Publications on behalf of the European Geosciences Union.

Abstract

Quantifying the impact of rotational Raman scattering (RRS) on the O_2 A- and B-bands is important as these bands can be used for cloud- and aerosol-characterization for trace-gas retrievals including CO_2 and CH_4. In this paper, we simulate the spectral effects of RRS for various viewing geometries and instruments with different spectral resolutions. We also examine how aerosols affect the amount of RRS filling-in. We show that the filling-in effects of RRS are relatively small, but not negligible, in these O_2 absorption bands, particularly for high spectral resolution instruments. For comparison, we also compare and contrast the spectral signatures of RRS with those of terrestrial chlorophyll fluorescence.

1 Introduction

Near InfraRed (NIR) retrievals of trace-gas concentrations, such as of CO_2 and CH_4, as well as terrestrial chlorophyll fluorescence often use information derived from O_2 A- and B- absorption band measurements (e.g., Reuter et al., 2010; Yoshida et al., 2011; Crisp et al., 2004; Guanter et al., 2010). Additive signals that contribute to satellite-measured top-of-the-atmosphere (TOA) radiance in the O_2 A- and B-bands can bias these retrievals. One type of additive signal that can produce a filling-in of deep telluric NIR absorption features, such as those in the O_2 A- and B-bands, is atmospheric rotational-Raman scattering (RRS) of N_2 and O_2 molecules. RRS has been neglected in the NIR spectral region, because the amount of atmospheric molecular scattering is low at these wavelengths. To the best of our knowledge, RRS effects in the O_2 A- and B-bands have not been quantified in the literature. However, RRS effects are worthy of consideration owing to the high accuracy and precision requirements placed on CO_2 retrievals to be used for carbon assessment (e.g., Crisp et al., 2004).

Recent advances in the satellite retrieval of chlorophyll fluorescence in the NIR (Guanter et al., 2007, 2010, 2012; Joiner et al., 2011, 2012; Frankenberg et al., 2011b)

AMTD
5, 8789–8813, 2012

also call into question the role of RRS in this spectral region. For example, Joiner et al. (2011, 2012) examined the filling-in of various solar Fraunhofer lines in the NIR and found the effects to be generally small, but not negligible. Frankenberg et al. (2012) showed that systematic biases in the CO_2 mixing ratio can be as large as 1 ppm if chlorophyll fluorescence in the O_2 A-band, amounting to 1 % to the continuum level radiance, is neglected. While RRS was not considered in that paper, it produces a similar spectral effect on TOA radiances and should be examined.

In this paper, we detail the effects of RRS in the O_2 A- and B-bands under various conditions. For comparison, we simulate the effects of chlorophyll fluorescence in the same bands. We also examine the impact of aerosol and thin clouds on both RRS and fluorescence additive signals within these absorption bands.

2 Radiative transfer simulations

2.1 Rotational Raman scattering

We compute inelastic rotational-Raman scattering (RRS) in the O_2 A- and B-bands using the LInearized Discrete Ordinate Radiative Transfer (LIDORT-RRS) code (Spurr et al., 2008). LIDORT-RRS allows for accurate radiative transfer (RT) calculations in the presence of cloud/aerosol scattering. Oxygen absorption coefficients are calculated using a line-by-line code with spectroscopic absorption line parameters from the HIgh-resolution TRANsmission (HITRAN) molecular absorption database (Rothman et al., 2005) and the Voigt line shape profile. A single mid-latitude profile of temperature/pressure was used in the computation of the absorption coefficients.

For reference, Fig. 1 shows the rotational-Raman spectra of N_2 and O_2 computed as in Joiner et al. (2011) at a temperature of 273 K for an excitation wavelength near the O_2 A-band (760 nm). The rotational-Raman lines peak at around ±3–4 nm from the excitation wavelength and extend to approximately ± 10 nm. Therefore, the spectral response of RRS is not the same as that for an additive signal as is more the

AMTD
5, 8789–8813, 2012

case for chlorophyll fluorescence. However, the overall spectral effects of the RRS and fluorescence signals are similar, as will be shown below.

2.2 Chlorophyll fluorescence

The TOA fluorescence signal is calculated approximately using the quasi-single scattering approximation, i.e.,

$$I_f(\lambda) = I_{f0}(\lambda)\exp[-(\tau_a(\lambda)+\tau_s)/\cos(\theta)], \quad (1)$$

where I_{f0} is the fluorescence radiance at the surface (assumed to be isotropic), θ is the viewing zenith angle (VZA), $\tau_a(\lambda)$ is the absorption optical thickness of the atmosphere, and $\tau_s = \tau(1-g)$ is the scaled aerosol optical thickness, where τ is the aerosol optical thickness, assumed to be spectrally independent within the O_2 A-band, g is the asymmetry parameter of the aerosol phase function. For non-absorbing wavelengths, this approach is applicable for low values of the scaled scattering optical thickness.

The far-red fluorescence radiance feature at the surface is approximated by a Gaussian function, i.e., $I_{f0}(\lambda) = I_m \exp[-(\lambda-\lambda_0)^2/(2\sigma^2)]$, where $\lambda_0 = 736.8$ nm and $\sigma = 21.2$ nm for the O_2 A-band and $\lambda_0 = 685.2$ nm and $\sigma = 9.6$ nm for the O_2 B-band. We assume $I_m = 2\,\mathrm{mW\,m^2\,sr^{-1}\,nm^{-1}}$ at a solar zenith angle (SZA) of 45° for both bands. This gives a surface fluorescence radiance at 762 nm of $\sim 1.0\,\mathrm{mW\,m^2\,sr^{-1}\,nm^{-1}}$. This value of surface fluorescence radiance near the O_2 A-band is typical of observed terrestrial chlorophyll fluorescence values within the O_2 A-band spectral range and corresponds to approximately 1 % of the continuum level radiance at a surface albedo of 30 %.

2.3 Satellite instrument simulation

Quasi-monochromatic computations are carried out at a spectral sampling of 0.01 nm, that of the solar irradiance reference spectrum from Chance and Kurucz (2010). For evaluation purposes, we also performed a limited number of RT computations with

AMTD
5, 8789–8813, 2012

higher spectral sampling (0.001 nm) using the solar irradiance spectrum from kurucz.harvard.edu/sun/irradiance2005/irradthu.dat. The latter sampling requires an order of magnitude more computational resources for a given calculation.

Computed TOA radiances are convolved with Gaussian response functions having various values of the full-width at half-maximum (FWHM). The chosen FWHMs (0.03, 0.1, 0.5, and 1 nm) are representative of existing and future satellite instruments. They include high spectral resolution instruments such as the Fourier Transform Spectrometer (FTS) on the Japanese Greenhouse gases Observing SATellite (GOSAT) (Kuze et al., 2009) and the Orbiting Carbon Observatory 2 (OCO-2) (Crisp et al., 2004) and moderate spectral resolution instruments such as the SCanning Imaging Absorption spectroMeter for Atmospheric CHartographY (SCIAMACHY) instrument aboard the EnviSat (Gottwald et al., 2006) and the proposed FLourescence EXplorer (FLEX) (Rascher, 2007).

For reference, the solar irradiance spectrum convolved with the chosen response functions is shown in Fig. 2 in the spectral ranges selected around the O_2 A- and B-bands. It is seen that these spectral ranges contain several deep Fraunhofer lines. RRS fills in Fraunhofer lines due to spectral transport of energy from wavelengths in the vicinity of the lines. The filling-in is larger for deeper lines.

2.4 Surface specification and viewing geometries

For simplicity, we assumed a spectrally-independent Lambertian surface with reflectivities R = 30 % in the O_2 A-band and 5% in the O_2 B-band. These values are typical for vegetated surfaces. The TOA simulations are performed for three solar zenith angles (20°, 45°, and 70°) at various viewing zenith and azimuth angles appropriate for typical satellite observations.

AMTD
5, 8789–8813, 2012

3 Results and discussion

3.1 RRS effects for molecular scattering only

Figure 3 shows TOA elastic (I_e) and inelastic (I_{rrs}) RRS radiances calculated for SZA = 45° and observation at nadir for a clean sky (i.e., aerosol free). The inelastic RRS radiances are small as compared with the elastic radiances, I_e. The inelastic radiances are positive within the O_2 A-band where the amount of outgoing Raman scattered light from those wavelengths is less than the amount of incoming Raman scattered light from excitation wavelengths in the surrounding continuum. The reverse is true of wavelengths near to or in the shoulders surrounding the O_2 A-band.

Figure 4 shows the percent difference between the total and elastic (sun-normalized) radiances, also known as the filling-in factor, i.e., $I_{rrs}/I_e * 100$ (in %). Within deep telluric absorption lines where elastic radiances are small, the filling-in can be as large as 2 % for high spectral resolution instruments. Note that the filling-in does not decrease linearly with increasing FWHM within the O_2 A-band. For relatively low-resolution instruments (FWHM = 1 nm), the maximum filling-in is < 0.2 %. A comparison the RRS filling-ins computed using the reference solar irradiance from Chance and Kurucz (2010) and the solar irradiance with higher spectral sampling from kurucz.harvard.edu/sun/irradiance2005/irradthu.dat shows that differences between them are generally very small except for a few narrow and deep Fraunhofer lines beyond the O_2 A-band. The use of the higher spectral sampling solar irradiance produces larger values of the filling-in of those Fraunhofer lines (Fig. 5).

The RRS filling in the O_2 B-band is shown in Fig. 6. It can be seen that values of the RRS filling-in in the O_2 B-band are significantly lower than in the O_2 A-band despite the fact that there is more atmospheric scattering at the O_2 B-band. This is explained by the fact that absorption lines in the O_2 A-band are much deeper than in the O_2 B-band. Thus, the filling-in from Raman scattered light coming from excitation wavelengths in the surrounding continuum in terms of percent of normalized radiance is larger in the

AMTD
5, 8789–8813, 2012

O_2 A-band than in the O_2 B-band. The remainder of the paper will therefore focus primarily on filling-in of the O_2 A-band.

3.2 RRS viewing angle dependences

Figure 7 is similar to Fig. 4 but shows the spectral RRS filling-in in the O_2 A-band for SZA = 70°. At high spectral resolution, the increase from SZA = 45° to SZA = 70° at the wavelength with the largest filling-in is about a factor of 2. At lower spectral resolution (FWHM = 1 nm) the increase is approximately a factor of 4.

The VZA dependence of the RRS filling-in at the wavelength with the largest filling-in is shown in Fig. 8 for SZA = 45° and 70° at azimuth angle of 90°. The RRS filling-in increases with VZA owing to increased photon path lengths and thus increased probability of Raman scattering.

3.3 Comparison of RRS and fluorescence spectral signatures

Figure 9 shows the TOA fractional fluorescence radiance (defined as a ratio of fluorescence radiance to elastic radiance) computed for SZA = 45° and observation at nadir. For this viewing geometry and a substantial amount of assumed chlorophyll fluorescence ($2\,mW\,m^{-2}\,sr^{-1}\,nm^{-1}$ at the peak), the fractional fluorescence signal is significantly higher than that of RRS. The spectral effects of fluorescence and RRS filling-in are similar within this spectral region though some small differences are observed. For example, the fluorescence spectral response contains a slight tilt across this wavelength range owing to the Gaussian shape of the emission feature. The relative ratio of fluorescence to RRS filling-in within the O_2 A-band depends upon the FWHM. At high spectral resolution (FWHM = 0.03 nm), the fractional fluorescence signal exceeds that of RRS by a factor of about 2 at the center of the O_2 A-band, while at FWHM = 1.0 nm, fluorescence is larger than RRS by a factor of 6.4. Note that we have subtracted the fluorescence signal in the continuum from the total fluorescence signal to enhance the spectral comparison with RRS effects.

AMTD
5, 8789–8813, 2012

A direct comparison of the spectral RRS and fluorescence signals is shown in Fig. 10 for FWHM = 0.1 nm. Again for clarity, the fluorescence spectral response has been normalized with respect to the continuum value. Two values of the peak surface fluorescence radiance are used for the comparison, our basic value of 2 mW m^2 sr^{-1} nm^{-1} and and a second lower by a factor of 4. At the lower surface fluorescence radiance, the fractional RRS and fluorescence signals are similar. However, there are some subtle differences.

The fractional fluorescence radiance in the O_2 B-band is shown in Fig. 11. The O_2 B-band is spectrally located nearby the peak of 685 nm fluorescence emission feature. Therefore, the total percentage contribution of fluorescence to the TOA radiance is much higher in the O_2 B-band as compared with the O_2 A-band. However, when the fluorescence signal is normalized with respect to the continuum, the relative fluorescence contribution to the TOA radiance in the O_2 B-band is somewhat lower than in the O_2 A-band. This is explained by deeper absorption lines in the O_2 A-band as compared with the O_2 B-band.

3.4 Aerosol and cloud effects on RRS

We carried out RT computations in the presence of aerosol/cloud with various optical depths and layer heights. Aerosol/cloud scattering is assumed to be in accordance with the Henyey-Greenstein (H-G) phase function with an asymmetry factor of 0.7 for aerosol and 0.85 for clouds. The simplified H-G phase function is adequate for our purpose of examining the qualitative effects of aerosol/cloud on RRS and fluorescence. We characterize the aerosol scattering effect on RRS (fluorescence) through a fractional difference of the TOA inelastic (fluorescence) radiance between aerosol and aerosol-free cases: $(I_r(\tau) - I_r(\tau = 0))/I_e(\tau = 0) * 100$ (in %) where I_r is either RRS I_{rrs} or fluorescence I_f radiance, τ is the aerosol optical depth. Figure 12 shows the fractional difference of the TOA inelastic radiance for a nonabsorbing aerosol plume with $\tau = 1.0$. The aerosol plume has a geometrical thickness of 1 km with a plume-top height of 3 km. In general, the aerosol effect on RRS is small. The presence of aerosol

AMTD
5, 8789–8813, 2012

increases inelastic radiance within oxygen absorption lines and decreases it beyond the absorption lines, i.e., in the continuum. The total aerosol effect is complex because of two opposing tendencies. Aerosol partly screens the atmosphere below the plume, decreasing photon path lengths. However, aerosol also increases photon path length owing to scattering between the bright ground and aerosol layer. The relative increase of the inelastic radiance owing to aerosol is larger for lower values of the FWHM. The aerosol effect on inelastic radiance depends on aerosol optical depth and height. RT computations for $\tau = 0.15$ show that the effect decreases by a factor of ~ 4 as compared with $\tau = 1.0$. Increase of the aerosol plume height also decreases the aerosol effect on RRS. For example, the aerosol effect at $\tau = 1.0$ decreases by a factor of ~ 1.8 when the aerosol height increases from 3 km to 10 km.

We looked at the cloud effect on RRS in terms of the maximum of the fractional inelastic radiance difference between cloudy and cloud-free cases. The presence of low altitude clouds substantially increases the cloud effect on RRS with increasing cloud optical depth (COD). Varying COD from 1 to 50 enhances the cloud effect on RRS by a factor of approximately 2. For brighter clouds, i.e., optically thicker clouds, the increase of photon paths above the cloud due to reflection from the cloud prevails over the decrease of RRS due to screening of the atmosphere below the cloud. The presence of high altitude clouds mostly decreases the cloud effect on RRS with increasing COD, i.e. screening of the atmosphere below the cloud plays the main role. However, optically thin clouds can slightly increase the cloud effect on RRS as compared with cloud-free case. This case is quite similar to the aerosol effect discussed in the previous paragraph.

The aerosol effect on the TOA fluorescence is quite simple: the presence of aerosol reduces the fluorescence signal according to Eq. (1). The fractional TOA fluorescence radiance difference between aerosol and aerosol-free cases, i.e., the difference normalized by the TOA radiance, significantly depends on wavelength. It is interesting that the presence of aerosol reduces the fractional fluorescence signal most substantially in the spectral range of strong absorption.

AMTD
5, 8789–8813, 2012

4 Conclusions

Our calculations show that RRS filling-in of telluric lines is comparable with small to moderate amounts of filling-in due to terrestrial chlorophyll fluorescence. RRS filling-in amounts to $<\sim 0.3\,\%$ of the continuum level radiance in the O_2 A-band for instruments with high spectral resolution (better than 0.1 nm). Neglect of RRS filling in the O_2 A-band may therefore lead to biases in satellite-retrieved CO_2 mixing ratios similar to effect of chlorophyll fluorescence shown in (Frankenberg et al., 2012). The RRS filling-in is also non-negligible for instruments with FWHM values of the order of 0.1 nm such as the proposed FLEX. The RRS filling-in of oxygen absorption lines increases for larger SZAs and VZAs. The percentage RRS filling in the O_2 B-band is less than in the O_2 A-band. The presence of a low altitude aerosol plume may slightly increase inelastic radiance and thus increase RRS filling-in. For an aerosol plume with $\tau = 1$ and height of 3 km, the fractional RRS filling-in increases by about 30 % in the center of the O_2 A-band as compared with the aerosol-free atmosphere.

Acknowledgements. Funding for this work was provided by the NASA Carbon Cycle Science program (NNH10DA001N) managed by Diane E. Wickland and Richard Eckman.

References

Chance, K. and Kurucz, R. L.: An improved high-resolution solar reference spectrum for Earth's atmosphere measurements in the ultraviolet, visible, and near infrared, J. Quant. Spectrosc. Radiat. Trans., 111, 1289–1295, 2010. 8792, 8794

Crisp, D., Atlas, R. M., Breon, F.-M., Brown, L. R., Burrows, J. P., Ciais, P., Connor, B. J., Doney, S. C., Fung, I. Y., Jacob, D. J., Miller, C. E., O'Brien, D., Pawson, S., Randerson, J. T., Rayner, P., Salawitch, R. J., Sander, S. P., Sen, B., Stephens, G. L., Tans, P. P., Toon, G. C., Wennberg, P. O., Wofsy, S. C., Yung, Y. L., Kuang, Z., Chudasama, B., Sprague, G., Weiss, B., Pollock, R., Kenyon, D., and Schroll, S.: The Orbiting Carbon Observatory (OCO) mission, Adv. Space Res., 34, 700–709, 2004. 8790, 8793

AMTD
5, 8789–8813, 2012

Crisp, D., Fisher, B. M., O'Dell, C., Frankenberg, C., Basilio, R., Bösch, H., Brown, L. R., Castano, R., Connor, B., Deutscher, N. M., Eldering, A., Griffith, D., Gunson, M., Kuze, A., Mandrake, L., McDuffie, J., Messerschmidt, J., Miller, C. E., Morino, I., Natraj, V., Notholt, J., O'Brien, D. M., Oyafuso, F., Polonsky, I., Robinson, J., Salawitch, R., Sherlock, V., Smyth, M., Suto, H., Taylor, T. E., Thompson, D. R., Wennberg, P. O., Wunch, D., and Yung, Y. L.: The ACOS CO_2 retrieval algorithm – Part II: Global XCO_2 data characterization, Atmos. Meas. Tech., 5, 687–707, doi:10.5194/amt-5-687-2012, 2012. 8790

Frankenberg, C., Butz, A., and Toon, G. C.: Disentangling chlorophyll fluorescence from atmospheric scattering effects in O_2 A-band spectra of reflected sun-light, Geophys. Res. Lett., 38, L03801, doi:10.1029/2010GL045896, 2011a.

Frankenberg, C., Fisher, J. B., Worden, J., Badgley, G., Saatchi, S. S., Lee, J.-E., Toon, G. C., Butz, A., Jung, M., Kuze, A., and Yokota, T.: New global observations of the terrestrial carbon cycle from GOSAT: Patterns of plant fluorescence with gross primary productivity, Geophys. Res. Lett., 38, L17706, doi:10.1029/2011GL048738, 2011b. 8790

Frankenberg, C., O'Dell, C., Guanter, L., and McDuffie, J.: Remote sensing of near-infrared chlorophyll fluorescence from space in scattering atmospheres: implications for its retrieval and interferences with atmospheric CO_2 retrievals, Atmos. Meas. Tech., 5, 2081–2094, doi:10.5194/amt-5-2081-2012, 2012. 8791, 8798

Gottwald, M., Bovensmann, H., Lichtenberg, G., Noel, S., von Bargen, A., Slijkhuis, S., Piters, A., Hoogeveen, R., von Savigny, C., Buchwitz, M., Kokhanovsky, A., Richter, A., Rozanov, A., Holzer-Popp, T., Bramstedt, K., Lambert, J.-C., Skupin, J., Wittrock, F., Schrijver, H., and Burrows, J. P.: SCIAMACHY, Monitoring the Changing Earth's Atmosphere, Published by DLR and Springer, doi:10.1007/978-90-481-9896-2, 2006. 8793

Guanter, L., Alonso, L., Gómez-Chova, L., Amorós-López, J., Vila-Francés, J., and Moreno, J.: Estimation of solar-induced vegetation fluorescence from space measurements, Geophys. Res. Lett., 34, L08401, doi:10.1029/2007GL029289, 2007. 8790

Guanter, L., Alonso, L., Gómez-Chova, Meroni, M., Preusker, R., Fischer, J., and Moreno, J.: Developments for vegetation fluorescence retrieval from spaceborne high-resolution spectrometry in the O_2-A and O_2-B absorption bands, J. Geophys. Res., 115, D19303, doi:10.1029/2009JD013716, 2010. 8790

Guanter, L., Frankenberg, C., Dudhia, A., Lewis, P. E., Gómez-Dans, J., Kuze, A., Suto, H., and Grainger, R. G.: Retrieval and global assessment of terrestrial chlorophyll fluorescence from GOSAT space measurements, Remote Sens. Environ., 121, 236–251, 2012. 8790

AMTD
5, 8789–8813, 2012

Joiner J., Bhartia, P. K., Cebula, R. P., Hilsenrath, E., McPeters, R. D., and Park, H.: Rotational-Raman scattering (Ring effect) in satellite backscatter ultraviolet measurements, Appl. Opt., 34, 4513–4525, 1995. 8791

Joiner, J., Yoshida, Y., Vasilkov, A. P., Yoshida, Y., Corp, L. A., and Middleton, E. M.: First observations of global and seasonal terrestrial chlorophyll fluorescence from space, Biogeosciences, 8, 637–651, doi:10.5194/bg-8-637-2011, 2011. 8790, 8791

Joiner, J., Yoshida, Y., Vasilkov, A. P., Middleton, E. M., Campbell, P. K. E., Yoshida, Y., Kuze, A., and Corp, L. A.: Filling-in of near-infrared solar lines by terrestrial fluorescence and other geophysical effects: simulations and space-based observations from SCIAMACHY and GOSAT, Atmos. Meas. Tech., 5, 809–829, doi:10.5194/amt-5-809-2012, 2012. 8790, 8791

Kuze, A., Suto, H., Nakajima, M., and Hamazaki, T.: Thermal and near infrared sensor for carbon observation Fourier-transform spectrometer on the Greenhouse Gases Observing Satellite for greenhouse gases monitoring, Appl. Opt., 48, 6716–6733, 2009. 8793

O'Dell, C. W., Connor, B., Bösch, H., O'Brien, D., Frankenberg, C., Castano, R., Christi, M., Eldering, D., Fisher, B., Gunson, M., McDuffie, J., Miller, C. E., Natraj, V., Oyafuso, F., Polonsky, I., Smyth, M., Taylor, T., Toon, G. C., Wennberg, P. O., and Wunch, D.: The ACOS CO_2 retrieval algorithm – Part 1: Description and validation against synthetic observations, Atmos. Meas. Tech., 5, 99–121, doi:10.5194/amt-5-99-2012, 2012.

Rascher, U.: FLEX – Fluorescence EXplorer: A remote sensing approach to quantify spatio-temporal variations of photosynthetic efficiency from space, Photosynth. Res., 91, 293–294, 2007. 8793

Reuter, M., Buchwitz, M., Schneising, O., Heymann, J., Bovensmann, H., and Burrows, J. P.: A method for improved SCIAMACHY CO_2 retrieval in the presence of optically thin clouds, Atmos. Meas. Tech., 3, 209–232, doi:10.5194/amt-3-209-2010, 2010. 8790

Rothman, L. S., Jacquemart, D., Barbe, A., Chris Benner, D., Birk, M., Brown, L. R., Carleer, M. R., Chackerian Jr., C., Chance, K., Coudert, L. H., Dana, V., Devi, V. M., Flaud, J.-M., Gamache, R. R., Goldman, A., Hartmann, J.-M., Jucks, K. W., Maki, A. G., Mandin, J.-Y., Massie, S. T., Orphal, J., Perrin, A., Rinsland, C. P., Smith, M. A. H., Tennyson, J., Tolchenov, R. N., Toth, R. A., Vander Auwera, J., Varanasi, P., and Wagner, G.: The HITRAN 2004 molecular spectroscopic database, J. Quant. Spectrosc. Radiat. Trans., 96, 139–204, 2005. 8791

AMTD
5, 8789–8813, 2012

Spurr, R. J. D., de Haan, J., van Oss, R., and Vasilkov, A. P.: Discrete ordinate radiative transfer in a stratified medium with first order rotational Raman scattering, J. Quant. Spectrosc. Radiat. Trans., 109, 404–425, 2008. 8791

Yoshida, Y., Ota, Y., Eguchi, N., Kikuchi, N., Nobuta, K., Tran, H., Morino, I., and Yokota, T.: Retrieval algorithm for CO_2 and CH_4 column abundances from short-wavelength infrared spectral observations by the Greenhouse gases observing satellite, Atmos. Meas. Tech., 4, 717–734, doi:10.5194/amt-4-717-2011, 2011. 8790

AMTD

5, 8789–8813, 2012

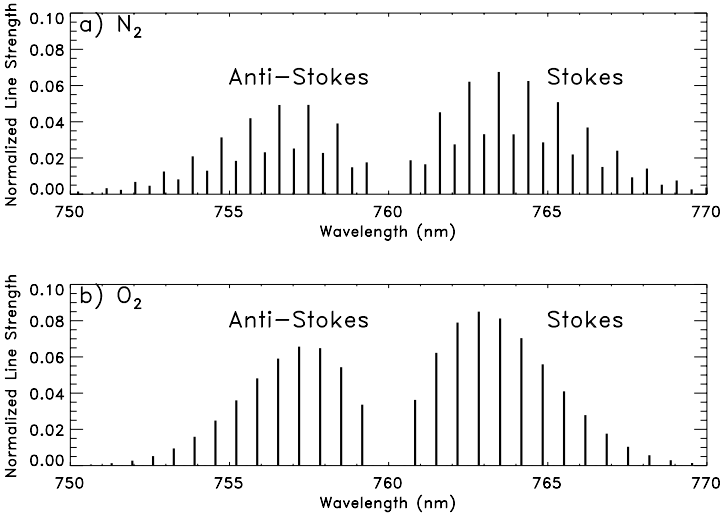

Fig. 1. Rotational-Raman spectra of **(a)** N_2 and **(b)** O_2 for excitation wavelength 760 nm. Line strengths are normalized such that the sum over all lines is equal to unity.

AMTD
5, 8789–8813, 2012

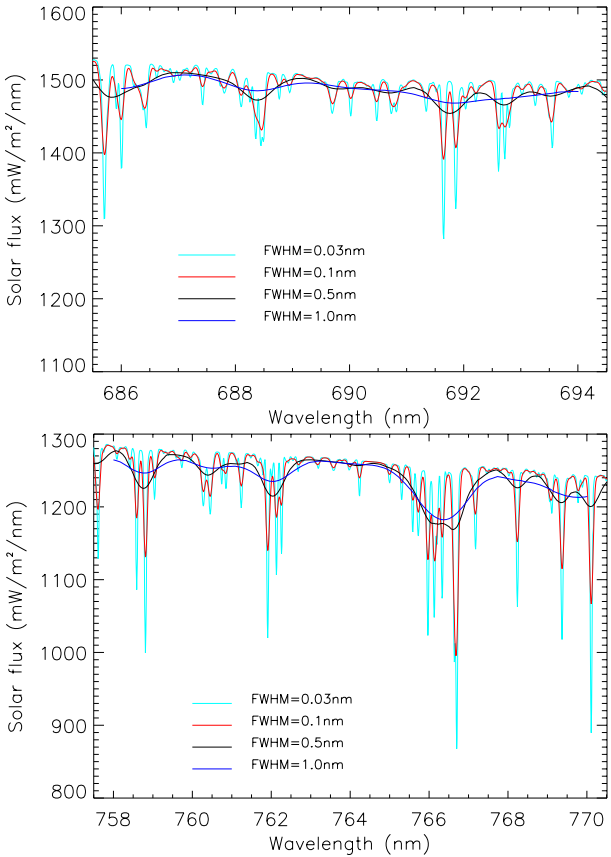

Fig. 2. Solar irradiance in the vicinity of O_2 B- (top) and O_2 A- (bottom) bands.

AMTD
5, 8789–8813, 2012

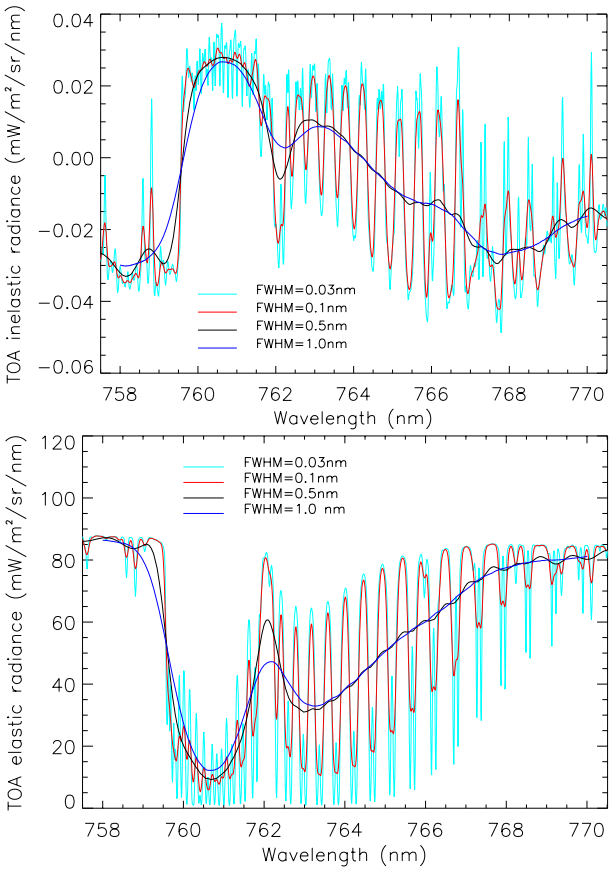

Fig. 3. TOA radiances, inelastic (top) and elastic (bottom) for SZA = 45° at nadir and a surface reflectivity of 0.3.

AMTD
5, 8789–8813, 2012

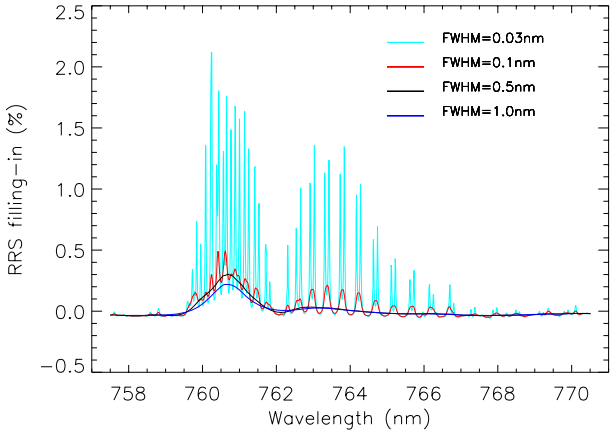

Fig. 4. Percentage filling-in from RRS for SZA = 45° at nadir and surface reflectivity of 0.3.

AMTD
5, 8789–8813, 2012

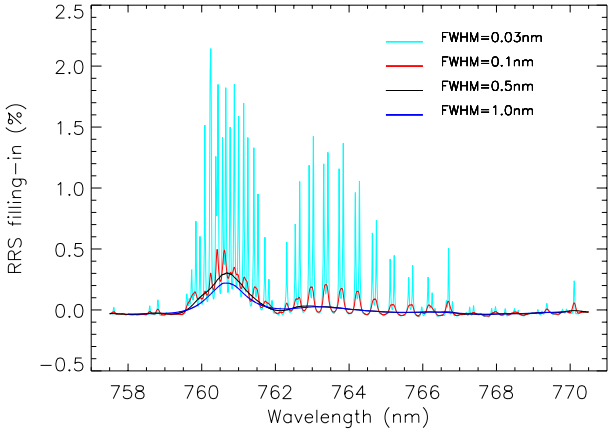

Fig. 5. Similar to Fig. 4 but computed with the higher spectral sampling solar irradiance (0.001 nm).

AMTD
5, 8789–8813, 2012

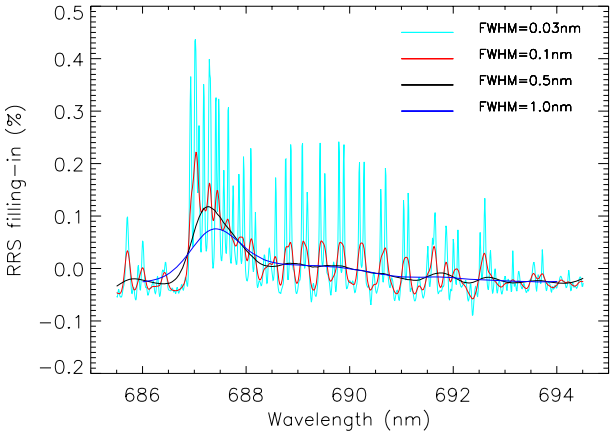

Fig. 6. Similar to Fig. 4 but for wavelengths in and surrounding the O_2 B-band and for a surface reflectivity of 0.05.

AMTD
5, 8789–8813, 2012

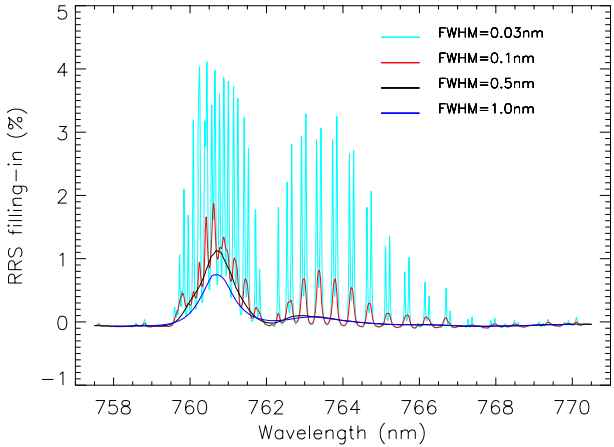

Fig. 7. Similar to Fig. 4 but SZA = 70°.

AMTD
5, 8789–8813, 2012

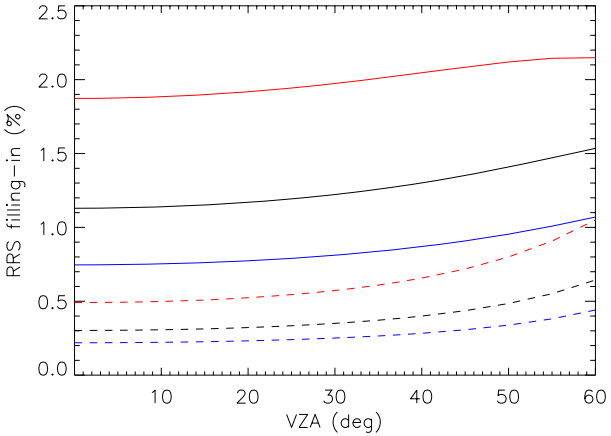

Fig. 8. Maximum percentage filling-in due to RRS as a function of VZA for SZA = 45° (dashed line) and 70° (solid line). Red: FWHM 0.1 nm; Black: FWHM 0.5 nm; Blue: FWHM = 1.0 nm.

AMTD
5, 8789–8813, 2012

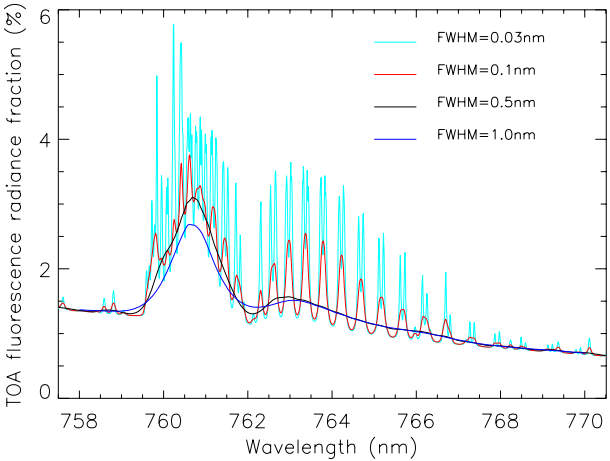

Fig. 9. Percentage contribution of fluorescence to TOA radiance for SZA = 45° at nadir and surface reflectivity of 0.3.

AMTD
5, 8789–8813, 2012

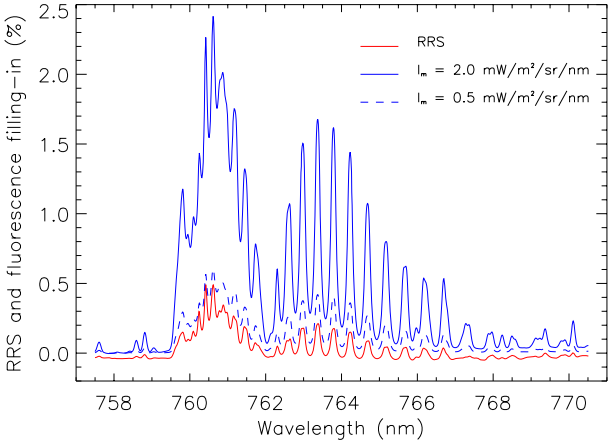

Fig. 10. Comparison of RRS (red line) and fluorescence (blue line) filling-in for FWHM = 0.1 nm; SZA = 45°. Observation at nadir; surface reflectivity 0.3.

AMTD
5, 8789–8813, 2012

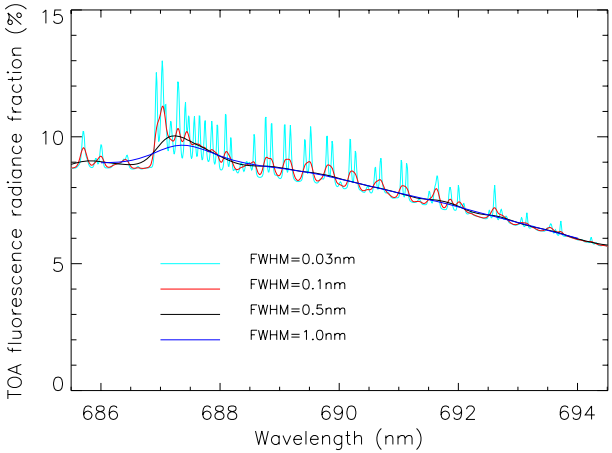

Fig. 11. Percentage contribution of fluorescence to TOA radiance for SZA = 45° at nadir and surface reflectivity of 0.05.

AMTD
5, 8789–8813, 2012

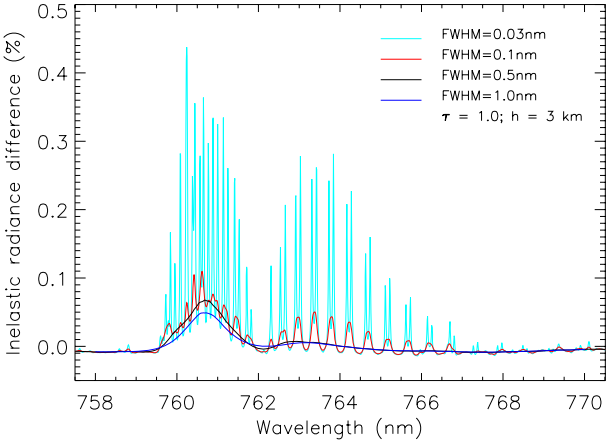

Fig. 12. Fractional inelastic radiance difference between aerosol loading with $\tau = 1.0$ and aerosol-free case. SZA = 45°; at nadir; surface reflectivity 0.3.

AMTD
5, 8789–8813, 2012